Pore-scale Conjugate Heat Transfer Analysis of Turbulent Flow over Stochastic Open-cell Metal Foams

Pore-scale Conjugate Heat Transfer Analysis of Turbulent Flow over Stochastic Open-cell Metal Foams

Alruwaili W., Jadidi M.*, Keshmiri A., Mahmoudi Y.**

Department of Fluids & Environment, University of Manchester, M13 9PL, United Kingdom

*Corresponding author: mohammad.jadidi@manchester.ac.uk

**Corresponding author: yasser.mahmoudi@manchester.ac.uk

Abstract

Fundamental understanding of turbulent flow and heat transfer in composite porous-fluid systems, which consists of a fluid-saturated stochastic open-cell metal foam and a flow passing over it, is crucial for fostering technological development in numerous applications such as transpiration cooling in aerospace, packed-bed thermal storage and thermal management of electronic devices. In this work, conjugate heat transfer simulations were adopted to explore the turbulent flow and heat transfer features in a composite porous-fluid system at the pore-scale. Simulations were performed to account for the influence of the blockage ratios (i.e., BR = 0.5, 0.8 and 1.0) on pressure drop and heat transfer rate by introducing a new concept called penetration cooling length. Furthermore, the effect of Reynolds numbers (i.e., Re = 1800, 3600 and 7200) at different blockage ratios was investigated in terms of pressure drop, fluid and solid temperatures, interstitial heat transfer coefficient, and flow leakage. Results indicate that for a fixed blockage ratio, as the Reynolds number increases by a factor of 3.0, there is a 14.9-fold increase in the pressure drop and a 2.9-fold increase in the interstitial heat transfer coefficient. Additionally, for a fixed Reynolds number, when the blockage ratio increases by a factor of 2.0, there is a 6.8-fold increase in the pressure drop and a 1.8-fold increase in the interstitial heat transfer coefficient. Flow visualisation indicated that the penetration cooling length is influenced by flow leakage from the porous-fluid interface. A correlation of IHTC is proposed based Reynolds number, blockage ratio and development length of the metal foam. Results show at small blockage ratios and low Reynolds numbers, a significant portion of the flow from the porous region leaves it to the clear region on top of the porous block. While, at high Reynolds numbers and large blockage ratios, the flow leakage is reduced. Additionally, for a low blockage ratio (BR<0.5), the amount of flow leakage depends on the Reynolds number, while it is independent of the Reynolds number for BR>0.8.

Keywords: Porous flow; Conjugate heat transfer; Penetration cooling length; Flow leakage; Interstitial heat transfer coefficient; Blockage ratio; Pore-scale simulation.

Nomenclature

Variable	Meaning	Unit
d	Pore diameter	m
h	Height of the porous block	m
H	Channel height	m
L_{foam}	Length of the porous block	m
p	Pressure	Pa
q_{wall}	Heat flux on the wall	W/m^2
Q_{in}	Flow rate that enters the porous block from the frontal face	m^3/s
Q_{fX}	Flow rate that leaks from the X-percentage of the porous-fluid interface	m^3/s
$Re = U_{in}h/\upsilon$	Reynolds number based on the inlet bulk velocity and porous block height	
$Re_d = U_{in}d/\upsilon$	Reynolds number based on the inlet bulk velocity and pore size	
T	Temperature	K
T_f	volumetric average temperature surrounding porous ligaments	
T_s	surface average temperature on porous ligaments walls	
$T^* = \dfrac{T - T_{in}}{T_{wall} - T_{in}}$	Non-dimensional temperature	–
u	Streamwise velocity component	m/s
U_{in}	Inlet bulk velocity	m/s
v	Vertical velocity component	m/s
X	Streamwise direction	m
Y	Vertical direction	m
Z	Spanwise (Lateral) direction	m
Symbol		
α_f	Thermal diffusivity of the working fluid	W/mK
Υ	Cooling angle	–
ε	Porosity	–
λ_s	Thermal conductivity	W/mK
ρ	Density	kg/m^3
υ	Molecular kinematic viscosity	m^2/s
Subscript		
f	Fluid	
in	Based on the inlet property	
s	Solid surface the porous ligaments	
$wall$	Based on the wall property	
Abbreviation		
$BR = h/H$	Blockage ratio, i.e., ratio of the porous block's height to channel height	–
CFD	Computational Fluid Dynamics	
CHT	Conjugate heat transfer	
$IHTC$	Interstitial heat transfer coefficient	W/m^{2}K
LES	Large Eddy Simulations	–
MF	Metal Foam	
Nu	Nusselt number	–
PPI	Pore density	
RANS	Reynolds Averaged Navier-Stokes	
SIMPLE	Semi-Implicit Method for Pressure Linked Equations	

1 Introduction

Composite porous-fluid systems, which consist of a fluid-saturated open-cell metal foam and a flow passing over it can be used in different applications including thermal energy storage [1-3], thermal management tools [4, 5] and catalytic reactors [6]. Having a high specific area has made the metal foams one of the best candidates in the case of thermal enhancement techniques [7]. Understanding the flow behaviour regarding the pressure drop and thermal field is essential to improving the efficiency of the thermal management system [8]. Although metal foams have outstanding heat dissipation, research has shown that they are associated with significant pressure drop, which results in a high reduction in the performance of the system [9-11]. In addition, the complexity of the flow inside the pores adds another challenge to obtaining a good understanding of the flow and thermal characteristics in composite porous-fluid systems [12].

Despite the clear relevance and importance of turbulent flow over metal foam to a wide range of applications, its full elucidation has been hindered by the lack of in-situ measurement of the flow properties (e.g., velocity and temperature); due to the inherent difficulties of flow measurement in small and intricate flow passages within the porous medium. Most of the attempts made to study experimental flow in metal foams were focused on some macroscopic average flow and thermal features [13-16]. The limited access to the interior of the metal foam prevents researchers from fully exploring the complexity of the flow structure inside [12].

To this extent, experimental studies on open-cell metal foam can be conducted with numerical methods to explore more about the flow characteristics. For example, Mancin, et al. [13] experimentally and numerically studied the geometrical parameters (porosity, pore density, and foam core height) of various metal foam specimens and found that the lower the porosity, the higher the overall heat transfer and in the interstitial heat transfer coefficient. Singh, et al. [17] conducted a comprehensive study involving both experimental and numerical approaches to analyze forced convective heat transfer. This investigation centred on aluminium foams with porosities ranging from 0.94 to 0.96 and varying pore densities between 10 and 40 PPI, all while subjecting them to the impingement of a 5 × 5 jet array. It was found that the enhancement in heat transfer performance is observed to be directly proportional to the rise in pore density for various jet array setups. Nie, et al. [18] carried out a numerical study on pressure drop and heat transfer mechanisms that found that the greater the pore density and the lower the porosity, the greater the pressure losses in the flow. Bai, et al. [19] analysed the influence of grading the porosity on the heat transfer coefficient and pressure drop. It was found that grading the porosity can improve the heat transfer and contribute to mitigating the pressure drop.

It has been observed that most of the previous publications focused on the geometric properties of the metal foam, whereas the blockage ratio (BR) and Reynolds number (Re) can have a significant influence on the flow behaviour and the overall thermal performance of composite porous-fluid systems [20]. Few experimental and numerical studies have been attempted on this matter in composite porous-fluid systems. Anuar, et al. [21] investigated the flow behaviour in a channel partially filled with three different metal foams' heights. It was concluded that after a specific foam length, a flow leakage towards the non-porous region was observed. This phenomenon was also noted for a specific PPI. By using LES pore-scale simulation, Jadidi, et al. [20] studied the turbulent flow over well-defined porous media shape at three Re numbers. According to the results, more than 52% of the fluid penetrating the porous region, leaves to non-porous region at the first part of the infinite porous media length. In their study, only one BR has been considered, and the effect of varying BR on the temperature distribution and flow was not explored.

Very recently, Jadidi, et al. [22] investigated the effect of Re numbers on the flow field in a composite porous-fluid system in which three Re numbers were considered. It was found that a huge amount of the flow escapes towards the non-porous region at the low Re number and this leakage decreases when increases Re number. The escape of flow or flow leakage from the porous region introduces significant complexities to the physics and flow characteristics, especially at the interface between the porous and non-porous regions [20]. Despite its importance, few studies have addressed the issue of flow leakage, and none have explored the impact of varying BRs through controlled adjustments of channel height on temperature distribution, interstitial heat transfer coefficient, and pressure drop. Consequently, a comprehensive investigation into these aspects is still lacking [22].

The numerical approach can be used especially at the pore-scale level since it has the capability to give detailed flow properties [23, 24]. The present work performs a conjugate heat transfer analysis of turbulent flow in a composite-porous fluid system with stochastic open-cell metal foam at the pore scale level. The main objectives are to investigate the simultaneous effects of the blockage ratio and Reynolds number on (i) Pressure drop and heat transfer coefficient in a composite-porous fluid system with stochastic open-cell metal foams, (ii) Important flow features, including flow leakage and the channelling effect, and thermal characteristics, such as fluid and solid temperature distributions. This is an unexplored aspect of turbulent flow behaviours and heat transfer characteristics in such systems. The investigation also explores a new concept for quantifying the flow penetration into the metal foam block (i.e., penetration cooling length) and its impact on the cooling effectiveness of the composite-porous fluid system.

2 Methodology

2.1 Computational domain and case description

The computational domain considered in this study is a horizontal channel filled with stochastic open-cell metal foam, which is located at the first part of the channel as shown in **Figure 1**. The channel width is $1.2h$ (22.9 mm), $24.3h$ which is 450 mm long and 18.5 mm highet. The 5 PPI metal foam used in this study has dimensions of 22.9 mm spanwise, 18.5 mm vertically, and 60 mm streamwise, respectively. In addition, the metal foam was cleaned with any incontiguous surfaces removed to create a higher-quality mesh. The side walls of the metal foam were kept in direct contact with the channel, so that the channel was fully filled with the metal foam and no escaping flows might be expected from anywhere except inside and above the metal foam in case of reducing the blockage ratio. Three blockage ratios (BRs) were considered in this study as follows: BR = 1.0 (where the channel is fully filled with metal foam and the metal foam height is equal to the channel height, $H = h$); BR = 0.8 (where the channel height is 1.25 times the metal foam height, H = 1.25h); BR = 0.5 (where the channel height is 2.0 times the metal foam height, H = 2.0h). In each case, the metal foam height (h) is constant and the channel height (H) is varied.

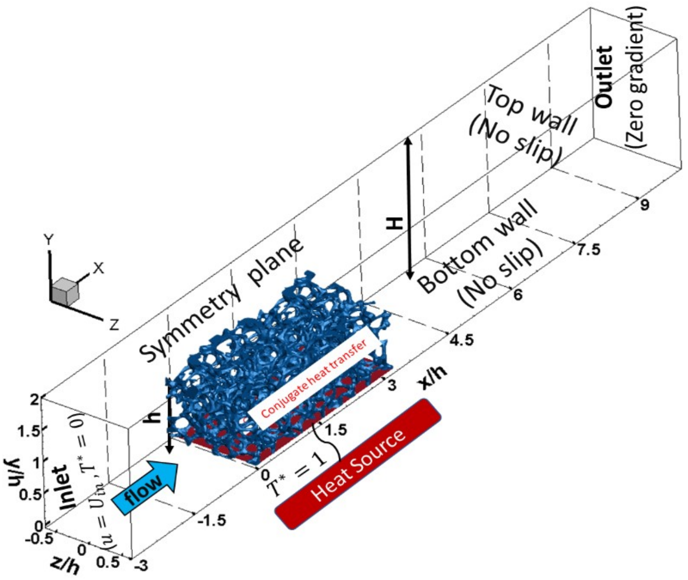

Figure 1 Computational domain and boundary conditions in a composite porous-fluid system for BR = 0.5.

2.2 Governing equations

The governing equations of the steady state RANS were solved in a CFD solver, STARCCM+ 2020.2.1 [25]. The finite volume method was considered to enable discretization, with pressure-velocity coupling obtained employing the SIMPLE scheme [25]. The flow was assumed to be incompressible, and the force of gravity was neglected. The governing equations for conjugate heat transfer (CHT) modelling, comprising mass, momentum, and temperature transport conservation principles, can be written as:

$$\frac{\partial u_i}{\partial x_i} = 0 \tag{1}$$

$$\frac{\partial}{\partial x_j}(u_i u_j) = -\frac{1}{\rho}\frac{\partial p}{\partial x_i} + \frac{\partial}{\partial x_j}\left([\nu + \nu_t]\frac{\partial u_i}{\partial x_j}\right) \tag{2}$$

$$\frac{\partial}{\partial x_j}(u_j T_f) = \frac{\partial}{\partial x_j}\left([\alpha_f + \alpha_t]\frac{\partial T_f}{\partial x_j}\right) \tag{3}$$

$$\frac{\partial}{\partial x_j}\left([\lambda_s]\frac{\partial T_s}{\partial x_j}\right) = 0 \tag{4}$$

where u_i is the velocity vector, ρ is the density of the fluid, p is the pressure, ν represents the kinematic viscosity. α_f and λ_s are the thermal diffusivity of the fluid phase and the thermal conductivity of the solid phase, respectively. T_f and T_s denote the temperature of the fluid and the solid phases, respectively. To calculate the interstitial heat transfer coefficient the following equation is used:

$$h_{sf} = \frac{q}{\langle T_s \rangle - \langle T_f \rangle} \tag{5}$$

where h_{sf} is the interstitial heat transfer coefficient ($IHTC$), q is the heat flux which represents the local heat flux transferred from the metal foam to the surrounding fluid. $\langle T_s \rangle$ and $\langle T_f \rangle$ are the spatial average temperatures of the solid and fluid, respectively, where the fluid temperature was calculated from the surrounding temperature of the ligaments since the conjugate heat transfer model has been activated the ligaments' temperature (solid phase temperature) is not constant.

2.3 Numerical method

The finite volume method was considered to enable discretization, with pressure-velocity coupling obtained employing the SIMPLE scheme [25]. A second-order upwind discretization scheme [25] was utilized to deal with the convective term, while convergence criteria were set to 10^{-6} for all residuals, along with the rate of heat transfer at the interface. A realizable $k - \varepsilon$ model [26] was used for the closure of the turbulent equations, as it has been reported in the literature that this has been found to perform efficiently for similar cases [12].

The inflow region was set to constant velocity and temperature, while a zero-pressure gradient was imposed for the outlet boundary. A no-slip boundary condition was set for the channel walls. The bottom surface of the metal foam is subjected to a constant temperature. The lateral walls were assumed to be symmetrical to reduce their impact on flow features. The channel walls in the upstream and downstream of the porous block are assumed to be adiabatic. Conjugate heat transfer analysis was performed to solve the temperature field in the solid ligaments of the metal foam. Several flow rates were studied by varying the Reynolds number (Re) defined based on the foam's height h and flow inlet velocity, i.e., Re = [3600, 1800, 7200]. The inlet air temperature was set to 300 K with dimensionless temperature T^* =0, and the heat source with T = 320 K (T^* =1) is imposed on the bottom wall boundary. At the coupling interface between the fluid and solid ligaments in the porous region, the fluid temperature was equal to the solid temperature.

Table 1 shows the numerical settings, boundary conditions and discretization schemes.

Table 1 Numerical settings, boundary conditions and discretization schemes.

Numerical settings	Boundary and model implemented
Pressure-velocity coupling	SIMPLE scheme
Turbulent	Realizable $k - \varepsilon$ model, y^+<2
Mesh size	10.1-12.2 million (depending on the case)
Lateral walls	Symmetry plane, zero temperature gradient
Top and bottom walls	Adiabatic & no-slip
Heat source on the bottom wall	Constant temperature T = 320 K ($T^* = 1$) & no-slip
Inlet	Constant temperature T = 300 K ($T^* = 0$) and uniform velocity
Solid material	Aluminum (Thermal conductivity = 237 W/m.K)
Working fluid	Air

Convective term	Second-order upwind discretization scheme
Diffusion term	Second-order central differencing scheme
Turbulence intensity	1%

Due to the complexity of the metal foam geometry and the tortuous paths it forms, an unstructured mesh based on the polyhedral grid was generated for the volume meshing using a surface constructed based on tetrahedral cells. Moreover. The cells at the fluid/solid interface must be conformal, as the size of the cells for each phase at the interface must be identical to allow the transmission stage of the heat transfer to be represented accurately. Another factor that must be considered is the growth rate of the cells: the transition of the cell size was set to 1.2 in all cases, while a local refinement was applied to the metal foam ligament to account fully for the solid phase. Three different mesh sizes were examined in this study: 5.3 million cells, 10.1 million cells, and 20.4 million cells. Average values of Y+ were kept below 2 to guarantee precise resolution of the laminar sublayer within the metal foam's interstitial spaces. The grid independence study showed that all three mesh sizes employed in this study exhibited close alignment and yielded nearly identical results. However, the 10.1 and 20.4 million cells demonstrated better capability in capturing the near-wall gradient. In addition, the average heat transfer coefficient was computed, and it has the value of 107.6 $\mathrm{W/m^2K}$, 110.84 $\mathrm{W/m^2K}$ and 111.58 $\mathrm{W/m^2K}$ for the mesh size of 5.3, 10.1 and 20.4 million cells, respectively. Based on these findings, the mesh consisting of 10.1 million cells was selected for further analysis in this study.

2.4 Validation

To validate the results, an experimentally based model, as devised by Mancin, et al. [27] was used to compare the pressure drop. As shown in **Figure 2** (a), the numerical results matched those of the experimental correlation model [27], offering evidence that the CFD model accurately predicts the pressure drop. To further validate the results, the average Nusselt number was compared against the available correlation in the literature in **Figure 2** (b). Due to the deficiency of the reported experimental studies on the heat transfer through the metal foam, correlations fitted with the pack beds have been used for different Reynolds ranges based on pores size (Re_d). It is observed that the current results are fitted within the range of the data predicted by those correlations and experiments. Furthermore, these correlations do not match each other, providing significant evidence of the complexity of flow within the porous structure. Variations in porosity, permeability, and flow conditions can lead to these discrepancies. Although it is possible to derive macroscopic quantities, there is no assurance of a strong correspondence with other findings due to differences in certain parameters as previously mentioned.

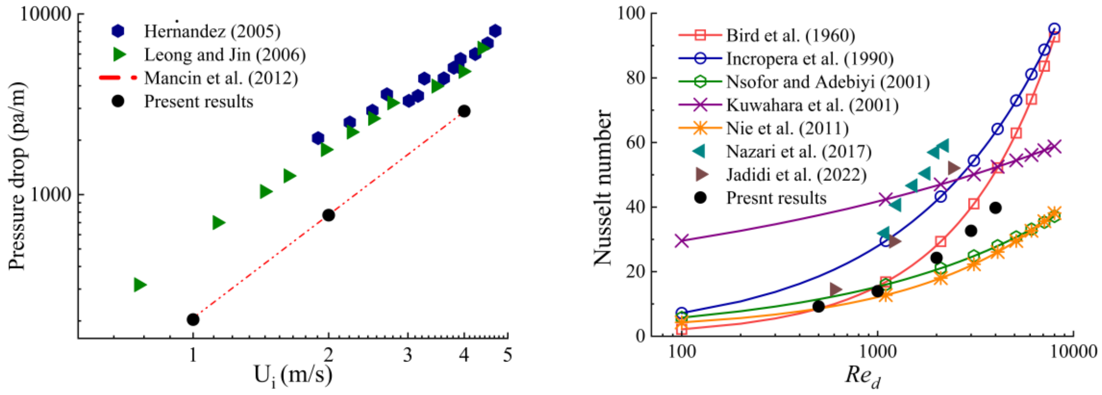

(a) Pressure drop **(b)** Nusselt number

Figure 2 Comparison of pressure drop and Nusselt number of current pore-scale study with the available measurements and correlations found in the literature; **(a)** Comparison of pressure drop in the composite porous-fluid system with Mancin, et al. [27], Leong and Jin [4] and Hernández [28]; **(b)** Comparison of Nu number with references: Byron Bird, et al. [29], Incropera, et al. [30], Nsofor and Adebiyi [31], Kuwahara, et al. [32], Nie, et al. [33], Nazari, et al. [13] and Jadidi, et al. [34].

3 Results and discussion

3.1 Flow field

Figure 3 shows the contours at z/h = 0 (middle plane section) of the non-dimensional vertical velocity (a-c) and non-dimensional streamwise velocity (d-f) of BR = 0.5, BR = 0.8 and BR = 1.0 at Re = 7200. The discussion of these results has been limited to the highest Re number (Re = 7200). No significant visual differences have been observed for the other Reynolds numbers. From **Figure 3** (a) it is seen that the flow is forced upward at the impinging of the metal foam as a high vertical velocity is noticed in this region. Moreover, the inability of the flow to pass fully through the metal foam can affect the momentum of the flow and reduce the cooling rate. At a low Reynolds number, special attention must be paid to the beginning of the metal foam, even if no significant difference is observed from these figures. This is because the momentum of the flow is weaker before it impinges on the porous block, which can cause a significant amount of flow leakage from the porous block. The low momentum induced at a low Reynolds number (Re) and blockage ratio (BR), in addition to the flow leakage, can directly affect the heat transfer performance of the metal foam. This will be discussed in Section 3.2. In addition, from **Figure 3** (d) it can be observed that the streamwise velocity is nearly doubled just above the interface between the porous and non-porous regions, indicating low momentum flow inside the metal foam.

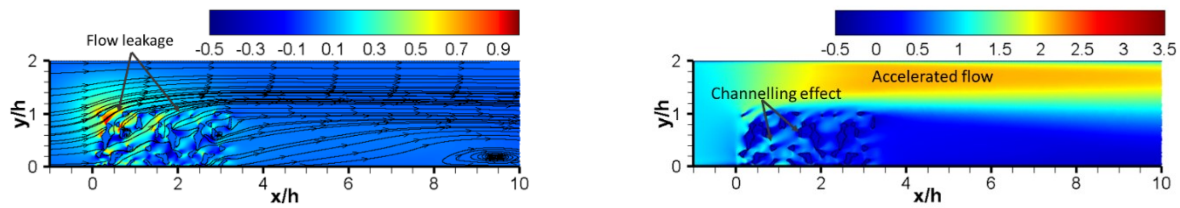

(a) Vertical velocity ($v^* = v/U_{in}$) for BR = 0.5 **(d)** Streamwise velocity ($u^* = u/U_{in}$) for BR = 0.5

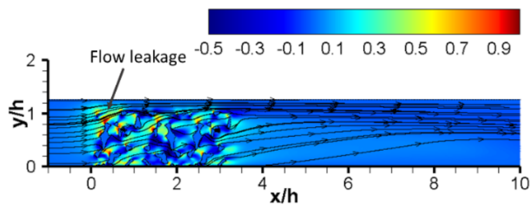

(b) Vertical velocity ($v^* = v/U_{in}$) for BR = 0.8

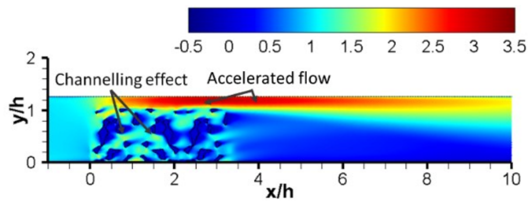

(e) Streamwise velocity ($u^* = u/U_{in}$) for BR = 0.8

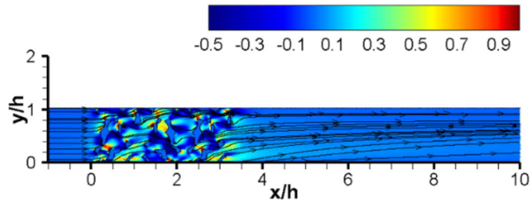

(c) Vertical velocity ($v^* = v/U_{in}$) for BR = 1.0

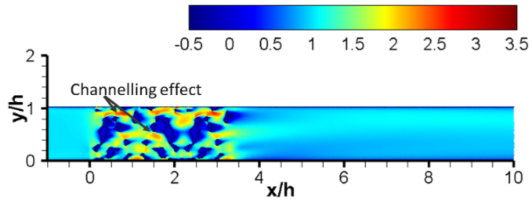

(f) Streamwise velocity ($u^* = u/U_{in}$) for BR = 1.0

Figure 3 Front view contours of velocity components at z/h = 0 (middle plane section) for different blockage ratios at Re = 7200.

The partial filling with BR = 0.8 in **Figure 3** (b and e) indicates that the flow can be accelerated to three times its upstream magnitude. This reduces the amount of flow that leaks out from the porous block, allowing high-momentum flow to penetrate the metal foam. In addition, the streamwise velocity is higher inside the tortuous path of the metal foam, which results in flow mixing with more heat that can be dissipated from the hot ligaments. It is worth noting that the improvement in heat transfer performance may come at the expense of increased pressure drop, as will be discussed later in the next section in **Table 2**. **Figure 3** (c and f) shows the case when BR = 1.0 means fully filling the channel with the porous block. A close look inside the pores can convey how the velocity increases significantly in comparison to BR = 0.5 and BR = 0.8. Despite having better momentum and mixing flow at BR = 1.0, the pressure drops are critical criteria that are considered in the design phase of the stochastic open-cell metal foam in thermal management systems and that will be quantified and discussed later in the following sections.

3.2 Flow leakage

The happening of flow leakage has been studied recently and more attention is being paid to the complex physics at the interface between the porous and non-porous regions [35]. However, all the pore-scale studies focus on the well-defined structure of the porous material or at a fixed BR [20, 22, 34, 35]. **Figure 4** shows the flow rates that enter and leak from the metal foam into the non-porous region along four streamwise positions 0.8h, 1.5h, 2.3h and 3.0h which enables the analysis of flow leakage for the two BRs, 0.8 and 0.5 at three Re numbers, 1800, 3600 and 7200. The methodology is adopted from Jadidi, et al. [20] as follows. $Q_{in} = \int_0^h \int_{-0.6h}^{0.6h} \langle \overline{u}(Y, Z) \rangle \, dZdY$, represents the absolute value of the flow that enters the metal foam. The flow rate the leaks out from the porous block along specified locations on streamwise direction at the interface between the porous and non-porous region can be quantified as $Q_{fX} = \int_0^{L_f} \int_{-0.6h}^{0.6h} \langle \overline{v}(X, Z) \rangle \, dZdX$. **Figure 4** (a) shows that the increases of Re number minimise the amount of the flow that can leak from the porous block even if the leakage is more than 50% for all the Re numbers at $1.5h$ which is considered an early stage of the porous block. In addition, the flow leakage can reach up to 70%, especially for low Reynolds numbers. This is because the low-momentum flow can easily leak from the porous block, where the huge free space of the non-porous region enables the flow leakage. These findings are in agreement with our previous findings by Jadidi, et al. [20] in the case of BR = 0.5. However, **Figure 4** (b) indicates an equal flow leakage from all the Re numbers at BR = 0.8 in which the dependency of Re number is no longer held when increasing the BRs. This behaviour can be attributed to the forced penetration of flow into the metal foam, with high-momentum flow in the non-porous region serving as a resistive layer, compelling the flow to traverse its path inside the pores, thus minimizing flow leakage.

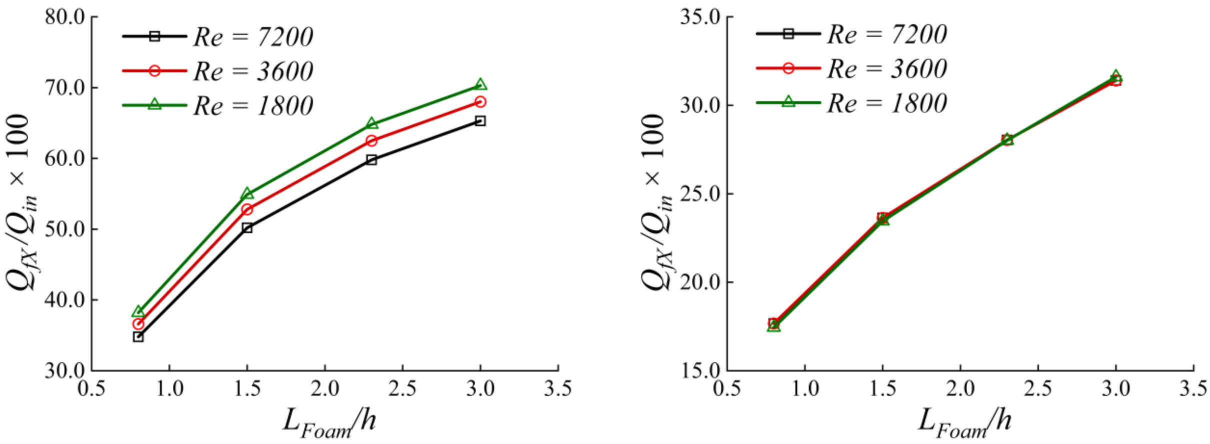

Figure 4 Flow leakage magnitude from porous-fluid interface along the streamwise direction on the porous-fluid interface; **Left**: BR = 0.5; **Right**: BR = 0.8.

3.3 Temperature field

Figure 5 shows the distribution of the heat flux on the bottom surface of a metal which is subjected to constant temperature for all cases considered in terms of Re number and BRs. The contour plots provided a detailed visualization of the thermal hydraulics of the flow field, highlighting the significant impact of both Re and BR on the distribution and intensity of heat flux. The white gaps in the visualization represent the ligaments of the foam, which significantly influence the heat transfer characteristics at the bottom surface. For lower Re number, as seen in **Figure 5** (a), (d), and (g), the heat flux contours are more uniform and less intense compared to higher Re, indicating a more stable and less turbulent thermal boundary layer. This stability is disrupted as Re increases, leading to more complex and intense heat flux patterns, as observed in **Figure 5** (b), (c), (e), and (f). The variation of BR from 0.5 to 1 also plays a crucial role, with a higher BR leading to a more pronounced disruption in the heat flux magnitude, suggesting a direct correlation between the spatial constraint imposed by the blockage and the resultant thermal behaviour.

Further analysis reveals that the interplay between Re and BR dictates the nature of thermal transport phenomena at the bottom surface. At a fixed Re, an increase in BR from 0.5 to 1 the convective heat transfer increases and the flow pattern clearly impacted by the obstruction of ligaments as it redirects the flow, hence, enhancing heat transfer rates. The transition from (g) to (i) at Re = 1800 show magnification of heat flux with increasing BR. Similarly, at a higher Re of 7200, as depicted in (b) and (c), the heat flux contours illustrate an increase the of complexity and intensity, underscoring the amplified influence of turbulent convective heat flux at higher flow velocities. These findings indicate that the control of heat flux distribution can be achieved through the manipulation of Re and BR, providing critical insights for optimizing thermal management strategies in various engineering applications.

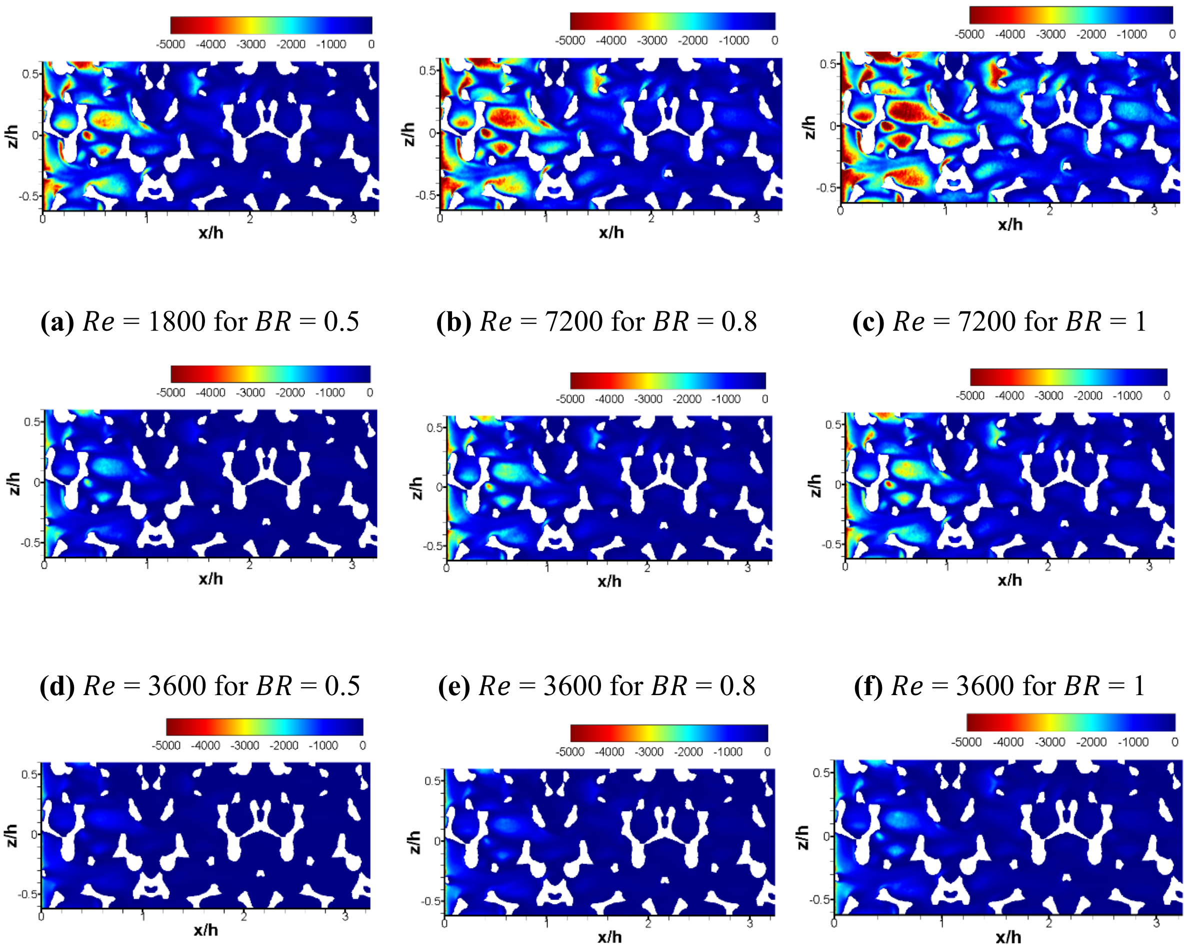

(a) Re = 1800 for BR = 0.5 **(b)** Re = 7200 for BR = 0.8 **(c)** Re = 7200 for BR = 1

(d) Re = 3600 for BR = 0.5 **(e)** Re = 3600 for BR = 0.8 **(f)** Re = 3600 for BR = 1

(g) Re = 1800 for BR = 0.5 **(h)** Re = 1800 for BR = 0.8 **(i)** Re = 1800 for BR = 1

Figure 5 Top view of the heat flux distribution on the bottom surface (y/h= 0) of a metal which is subjected to constant for all the cases considered.

Figure 6 shows the non-dimensional temperature (T^*) at z/h = 0 (middle plane section) for the fluid phase (a-c), and the solid phase (e-g) for BR = 0.5 at three Re numbers. In this case, a key parameter, the penetrating cooling length (PCL), has been introduced. It can be used as a measure of the thermal performance of the system together with BRs. Since the conjugate heat transfer model has been developed, the hot ligaments start losing their temperature when the cold air passes through the porous block, which in turn increases the air temperature. Therefore, with a constant-temperature heat source, the depth that air travels through until its temperature reaches the average temperature T^* = 0.5 is defined as the penetrating cooling length. The entrance centre of the porous block is used as a reference for the PCL in the streamwise direction. In addition, by using PCL, the gamma angel (γ) which equals to $\tan^{-1}((h/2)/\,PCL)$ can separate the porous block into separate regions to identify the parts or the segments that are not interacting with the cold air as a function of Re and BRs. Moreover, the higher the gamma value, the smaller the region that is being cooled effectively.

The mechanism of cooling the porous block, as mentioned earlier, is that the cold air enters the hot porous region and takes a tortuous path, causing a channelling effect [22, 34, 35]. This in turn dissipates some of the heat from the ligaments due to flow mixing. This can be seen in all the cases in this study. However, the effects of the Reynolds number and the BRs make the behaviours of the flow and the magnitude of the cooling quite distinct from each other. In **Figure 6** (a-c), the most extended PCL value can be observed at Re = 7200 in comparison to Re = 3600 and Re = 1800 at BR = 0.5.

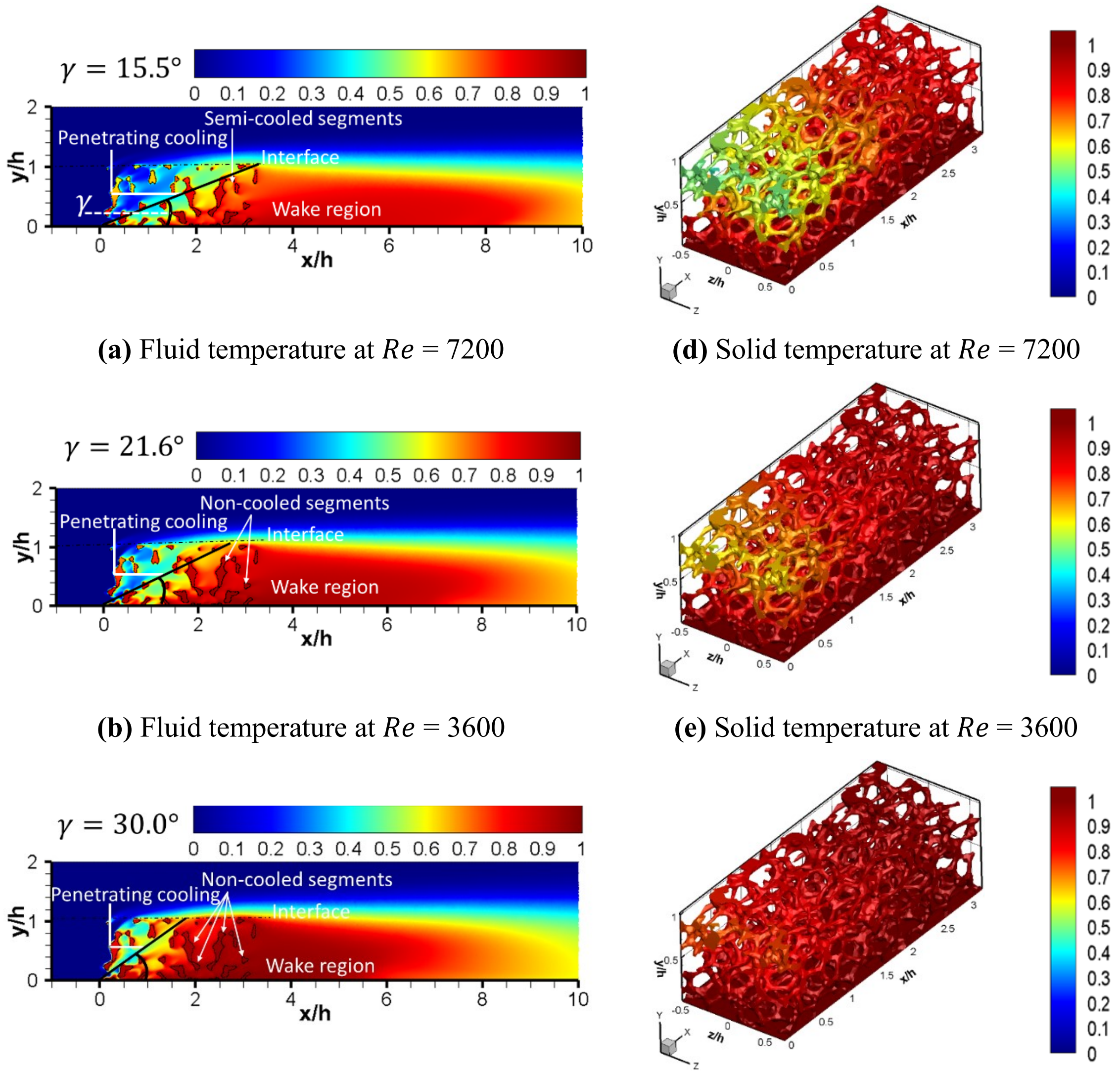

(a) Fluid temperature at Re = 7200 **(d)** Solid temperature at Re = 7200

(b) Fluid temperature at Re = 3600 **(e)** Solid temperature at Re = 3600

(c) Fluid temperature at Re = 1800 **(f)** Solid temperature at Re = 1800

Figure 6 (a-c) Front view of fluid temperature (z/h= 0); **(d-f)** 3D view of solid temperature for BR = 0.5 at three Re numbers.

Moreover, there is a considerable part of the porous ligaments that is non-cooled or experiences deficient cooling near the downstream region in both cases (Re = 3600 and Re = 1800), and it is even worse in the latter. The deficient and effective cooling regions can be separated by gamma angle, as can be seen in **Figure 6** (a–c), where γ = 30.0° in the case of Re = 1800, meaning a large number of ligaments remain non-cooled or semi-cooled. This can be explained by the fact that a significant amount of the flow leaks as it enters the porous block, as discussed in the flow leakage section. Increasing the BR has a drastic effect on heat transfer perofrmnace of the metal, especially at the first part of the foam and near the porous-fluid interface. Moreover, since the conjugate heat transfer model has been developed, the solid temperature varies according to the energy transfer between the cold air and hot ligaments as seen in **Figure 6** (e-f).

Figure 7 shows that by increasing the BR to 0.8 the PCL angle reduces to 11.83, which exposes the first top of the porous block near the porous-fluid interface to a temperature reduction. This can be attributed to the fact that the flow acceleration at the porous-fluid interface region enhances the heat dissipation from the solid part, which in turn raises the fluid temperature and increases the PCL.

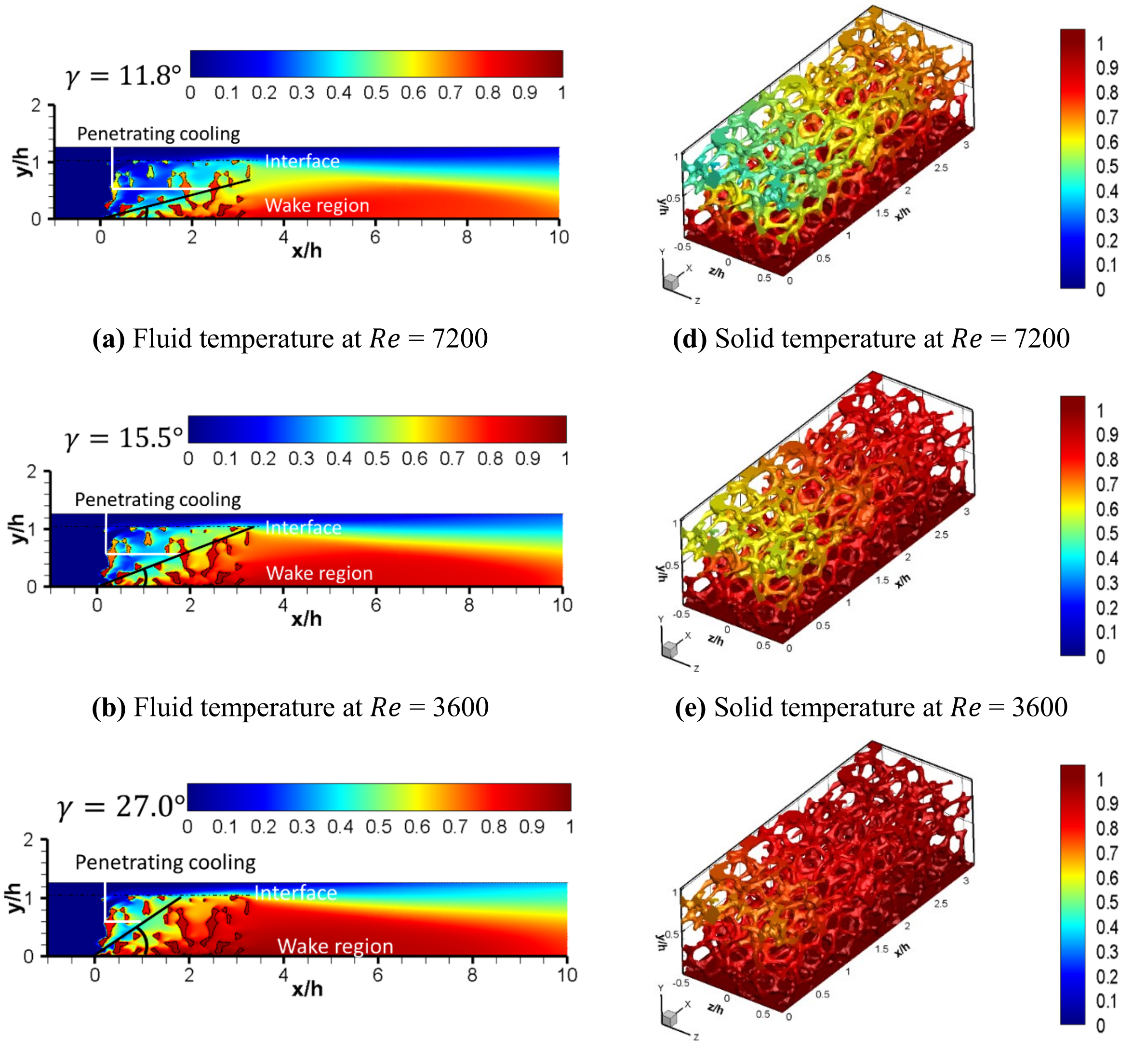

(a) Fluid temperature at Re = 7200 **(d)** Solid temperature at Re = 7200

(b) Fluid temperature at Re = 3600 **(e)** Solid temperature at Re = 3600

(c) Fluid temperature at Re = 1800 **(f)** Solid temperature at Re = 1800

Figure 7 (a-c) Front view of fluid temperature (z/h= 0); **(d-f)** 3D view of solid temperature for BR = 0.8 at three Re numbers.

The full blockage ratio case is shown in **Figure 8**, where the flow is forced to pass through the porous block. Interestingly, in the case of Re = 3600 and lower, the PCL angel is not affected in comparison to the other BRs. Consequently, the effect of a low Re number for the full blockage cases is less sensitive than its effect on the partial blockage cases. This could be due to the high inertial forces induced by the porous block which greatly affect the momentum of the pore flow.

Based on **Figures 6, 7, and 8**, we can deduce that there are three cases with almost the same penetrating cooling length (PCL) and temperature distribution: BR = 0.5 at Re = 7200, BR = 0.8 at Re = 3600, and

BR = 1.0 at Re = 1800. Therefore, for the optimal design of a thermal management system using metal foam, the trade-off design should be chosen, considering other factors such as pressure drop and required inlet power. Further discussion will be provided in the pressure drop and thermal performance analysis section.

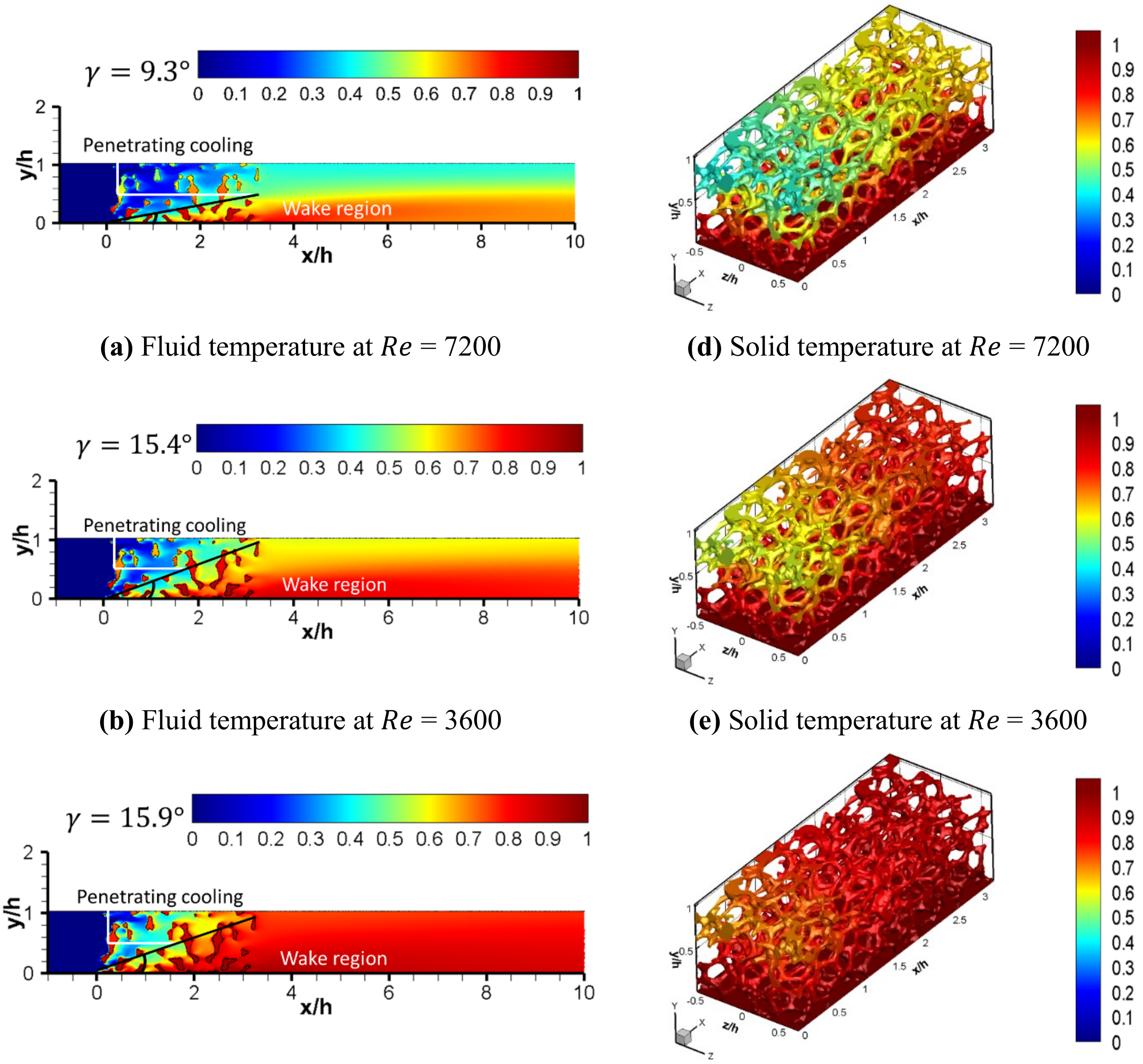

(a) Fluid temperature at Re = 7200 **(d)** Solid temperature at Re = 7200

(b) Fluid temperature at Re = 3600 **(e)** Solid temperature at Re = 3600

(c) Fluid temperature at Re = 1800 **(f)** Solid temperature at Re = 1800

Figure 8 (a-c) Front view of fluid temperature (z/h= 0); **(d-f)** 3D view of solid temperature for BR = 1.0 at three Re numbers.

3.4 Interstitial heat transfer coefficient ($IHTC$)

Figure 9 depicts the sectional average distribution of the local heat transfer coefficient ($IHTC$) along the streamwise direction. **Figure 9** (a-c) shows the $IHTC$ at constant Reynolds number (Re) for all blockage ratios (BRs), while **Figure 9** (d-f) shows the $IHTC$ at constant BR for different Re numbers. The impinging flow acts differently when it reaches the porous block, as a part of the flow leaks if the BR is less than 1.0. Consequently, at the windward face of the porous block, the $IHTC$ recorded the highest level in the case of a full blockage ratio. It can be seen from **Figure 9** (a-c) that although the start of the trend is nearly the same for all *BRs*, the case with *BR* = 1.0 possesses the highest value. Moreover, as the flow proceeds through the porous block, the trend of all cases is similar, where a fluctuating manner has been observed till the end of the porous block. These fluctuations are expected as the stochastic shape of the porous block can highly affect the *IHTC* where the flow velocity changes accordingly in the tortuous paths. In addition, the solid density can contribute to the magnitude of the *IHTC* where higher density ligaments increase the *IHTC*.

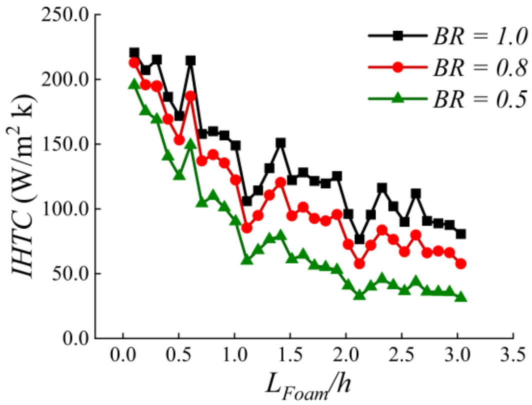

(a) Re = 7200

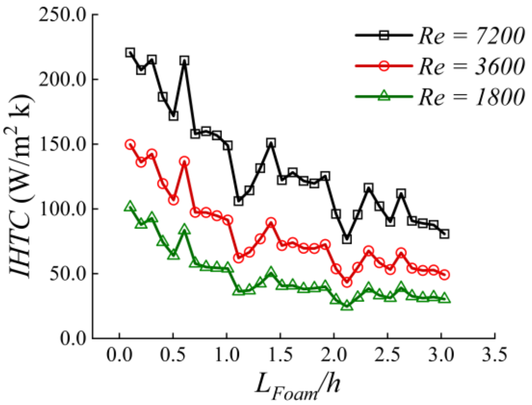

(d) BR = 0.5

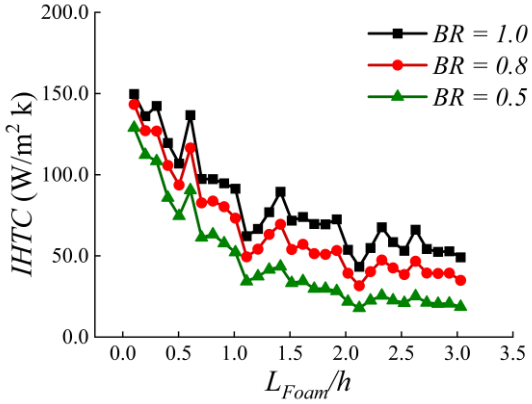

(b) Re = 3600

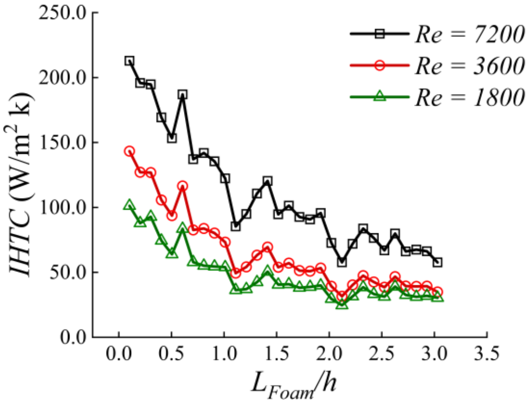

(e) BR = 0.8

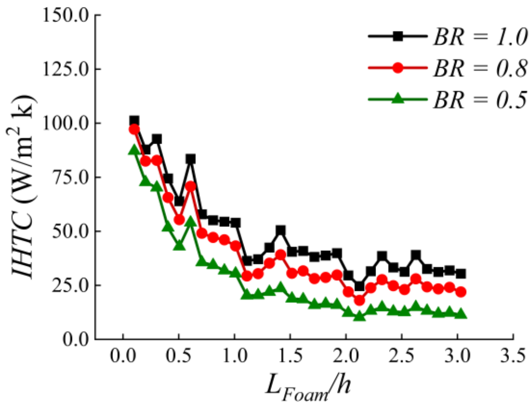

(c) Re = 1800

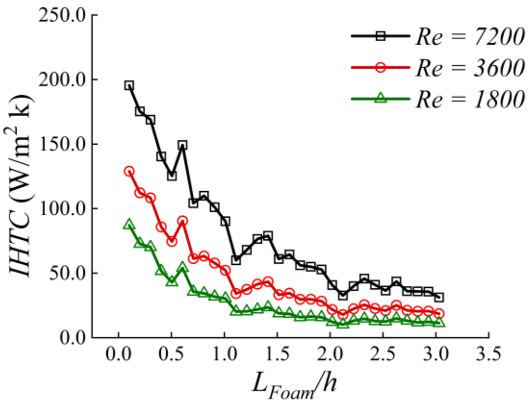

(f) BR = 1.0

Figure 9 Spatial spanwise average distribution of *IHTC* along the streamwise direction for **Left:** Three BRs at constant Re numbers; **Right**: Three Re numbers at constant BR.

Figure 9 (a-c) shows that the magnitude of the $IHTC$ at the same Reynolds number for all blockage ratios (BRs) initially starts close together. However, near the wake region, the difference between the magnitudes widens. This pattern is reversed when the Reynolds number is changed at the same BR, as shown in **Figure 9** (d-f). According to the results presented in **Figure 9** for airflow (with a constant Prandtl number) in an open-cell metal foam (with fixed porosity), the heat transfer coefficient is influenced by the *Re, BR*, and development length (*L/X*). Consequently, a correlation was established as follows $IHTC = 0.24.(L/X)^{-0.36}.(Re)^{0.71}.(BR)^{0.65}$. As can be observed in **Figure 9** and the proposed correlation by increasing the Re number and BR the IHTC enhances. However, the effect of Re number seems to be stronger for nearly 8%. Finally, the negative signs of the exponent of (L/x) indicates that the higher values of the *IHTC* takes place at the stagnation region and gradually decreasing towards the trailing edge of the metal foam.

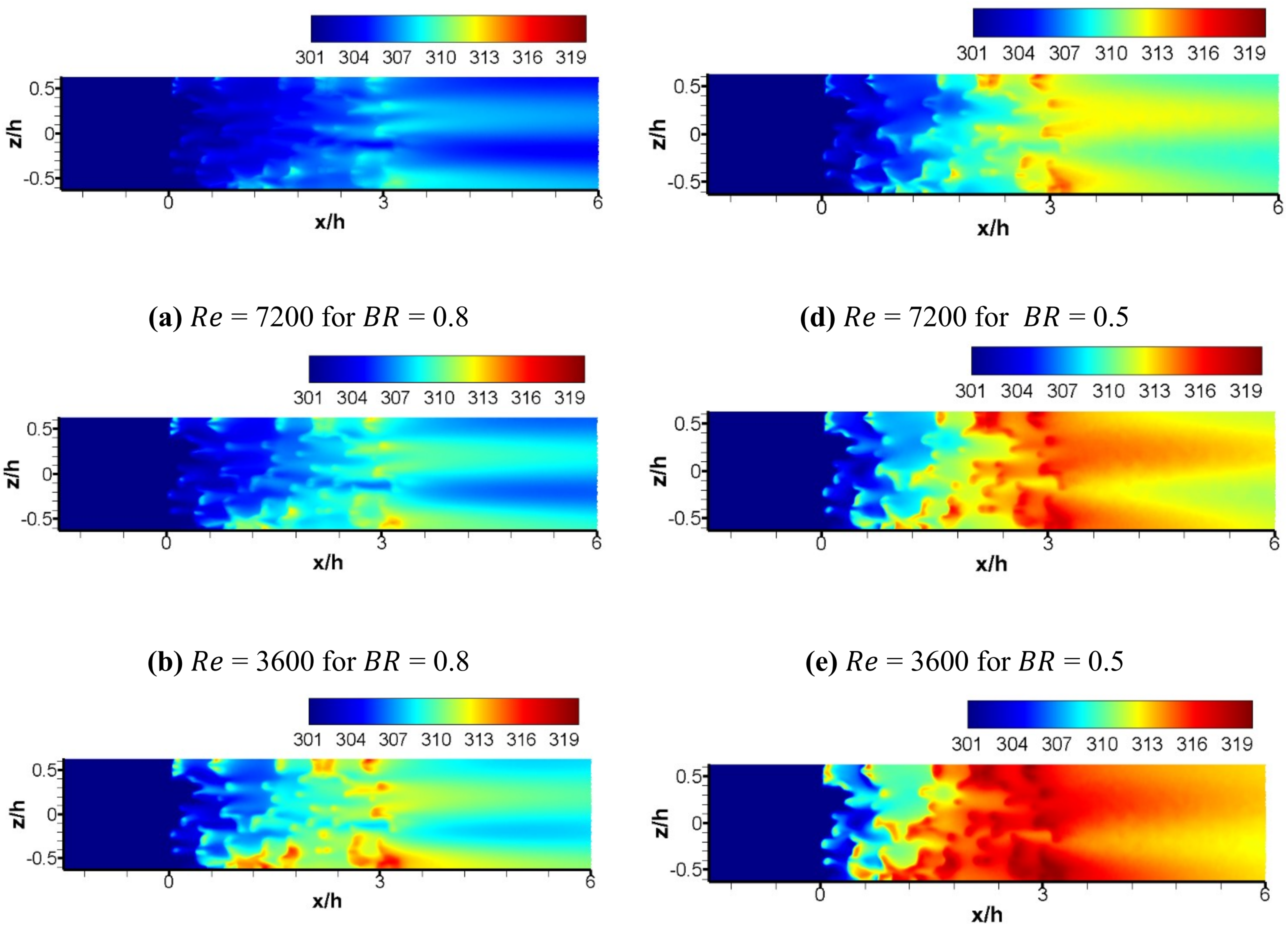

(a) Re = 7200 for BR = 0.8 **(d)** Re = 7200 for BR = 0.5

(b) Re = 3600 for BR = 0.8 **(e)** Re = 3600 for BR = 0.5

(c) Re = 1800 for BR = 0.8 **(f)** Re = 1800 for BR = 0.5

Figure 10 (a-c) Top view of the enthalpy (kJ/kg.k) (a-f) at the top interface of the metal foam (y/h= 1) of BR = 0.5, BR = 0.8 and at Re = 7200, Re = 3600 and Re= 1800 **(d-f)**

Figure 10 shows the contours of the enthalpy (a-f) at (y/h= 1) of BR = 0.5, BR = 0.8 and at Re = 7200, Re = 3600 and Re = 1800.The discussion of the flow leakage can be extended and explored more by relating flow energy to this phenomenon. The study underscores the profound impact of both Re number and BRs on the heat transfer process, revealing that these parameters significantly influence the total enthalpy at the interface. Careful examination of **Figure 10** (a) with high Re number indicates a lower enthalpy at the porous and nonporous interface than under any other conditions. This reduction in enthalpy is attributed to a smaller difference in local temperature between the fluid and the foam's ligaments, signifying effective cooling and consequently, reduced flow leakage. This observation not only highlights the efficiency of thermal exchange in high-velocity flows but also illuminates the intricate relationship between the Flow leakage and thermal performance of the unit.

The dependency of flow leakage on *Re* at high *BRs* is found to be sensible, a phenomenon illustrated as shown previously (**Figure 4**). In addition, decreasing the Re number amplifies the enthalpy at the trailing edge of the interface, attributed to an increased temperature difference, thereby increasing enthalpy exchange. Moreover, at a BR of 0.5 (Figures d-f), higher flow leakage correlates with a significant alteration in the foam's temperature distribution, notably near the trailing edge where cooling efficiency drops hence increases the enthalpy. These findings not only contribute to a deeper understanding of the dynamics of heat transfer in porous media but also pave the way for future research aimed at optimizing thermal management strategies in complex flow environments at different BRs.

Figure 11 shows the three-dimensional distribution of *IHTS* for all BRs at Re = 7200, Re = 3600 and Re = 1800. Due to the exposure of the flow stream and the low temperature, it is seen that the *IHTC* reaches its maximal value in the stagnation region for all the cases. However, the magnitude of the $IHTC$ can be distinguished for each blockage ratio, since BR = 1.0 and BR = 0.5 have the maximum and minimum values, respectively. In addition, in all the cases, the magnitude of the *IHTC* decreases through the foam until it reaches its minimal value at the trailing edge of the metal foam. This can be attributed to the reduction of the temperature difference between the ligaments and the surrounding passing flow. Furthermore, based on the Reynolds analogy [36] the $IHTC$ increases as the flow velocity rises. Therefore, the reduction of the velocity magnitude because of the metal foam can result in a deterioration of the thermal performance of the system.

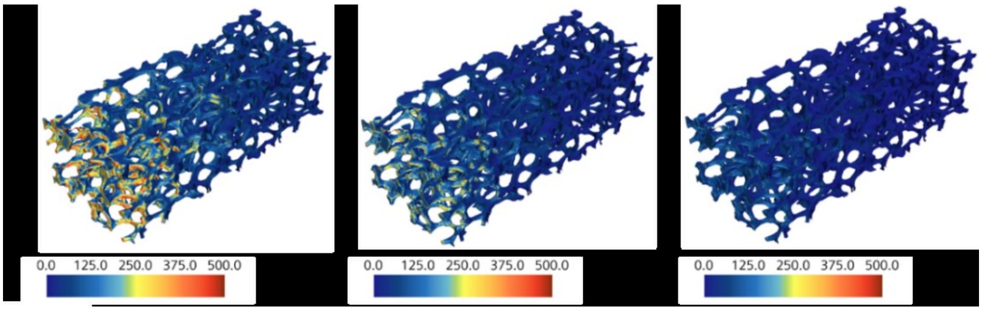

(a) Re = 7200 **(b)** Re = 3600 **(c)** Re = 1800

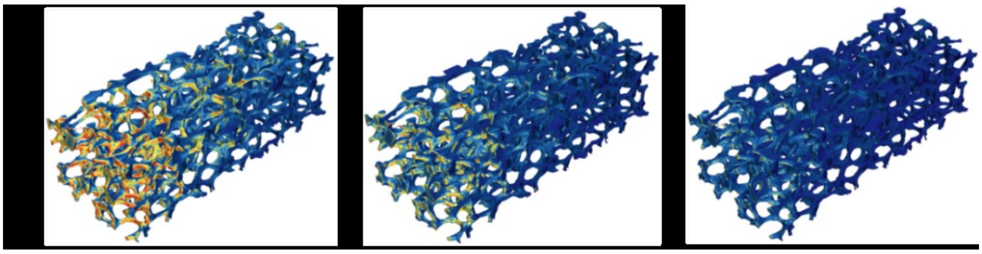

(d) Re = 7200 **(e)** Re = 3600 **(f)** Re = 1800

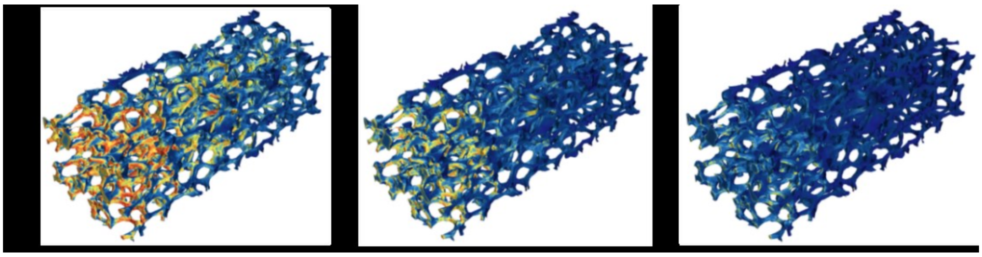

(g) Re = 7200 **(h)** Re = 3600 **(i)** Re = 1800

Figure 11 Interstitial heat transfer coefficient contour; **First row**: BR = 0.5; **Second row:** BR = 0.8; **Third row:** BR = 1.0.

3.5 Turbulent Kinetic energy

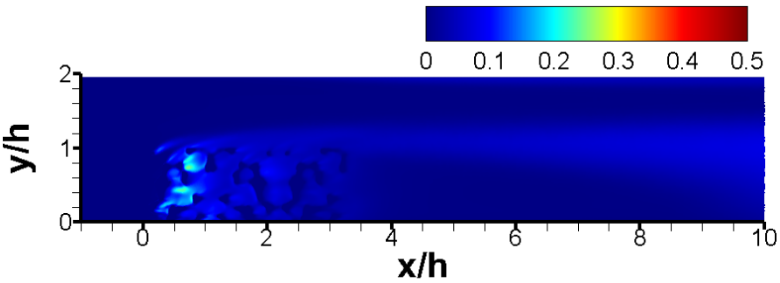

(a) BR = 0.5

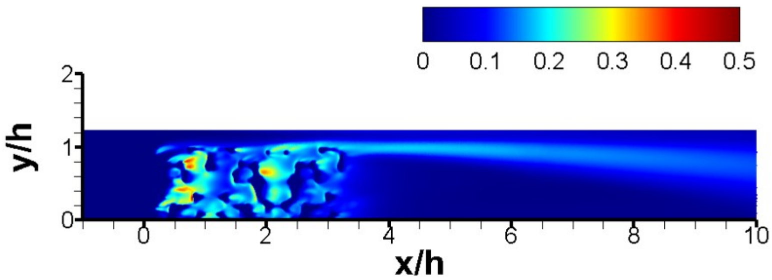

(b) *BR* = 0.8

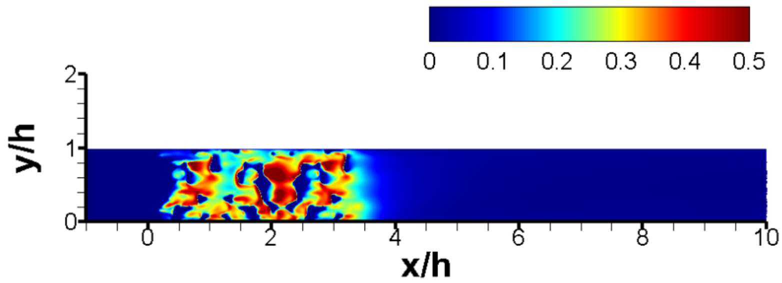

(c) *BR* = 1

Figure 12 (a-c) The normalised turbulent kinetic energy (TKE) TKE/U^2 at z/h = 0 for *BR* of 0.5, 0.8 and 1.0 at *Re* = 7200.

The distributions of turbulent kinetic energy (TKE) for *BR* of 0.5, 0.8 and 1 are shown in **Figure 12** at *Re* of 7200. Metal foams have a complex geometric structure that greatly affects the distribution of pressure, resulting in complicated pressure gradients and pore velocity variations that are closely related to the foam's structural characteristics. Remarkably, there is an obvious rise in TKE inside the foam pores, especially at the leading edge of the metal foam structure. Moreover, the figures clearly show that variation of *BR* influences the level of turbulent kinetic energy, where a higher *BR* is associated with increased flow turbulence. *BR* less than 1, it becomes evident that there are two distinct regions of interest. Firstly, a noticeable upsurge in the magnitude of TKE is observed at the leading edge. This surge indicates intensified fluid motion and turbulence magnitude within this region. As the flow progresses, it leads to the generation of turbulence at the interface, particularly notable when examining the location x/h = 2. This turbulence generation contributes to the magnify of TKE levels along the interface, with its effects extending towards the top of the wake region. However, it is noteworthy that in cases where *BR* = 0.5, the overall TKE budget is notably reduced compared to instances with higher *BR* values. Consequently, the flow tends to disperse further without experiencing significant reflection towards the interface, thereby influencing the distribution of TKE within the system.

3.6 Pressure drop and thermal performance analysis

Table 2 represents the penetration cooling length, average and normalised pressure drops, cooling angle and the mean value of *IHTC* for all the cases considered in this study. The average pressure drop was calculated utilizing taking absolute values at the leading edge and trailing edge of the metal foam. As it was concluded previously the higher the *BR* and *Re* number, the more heat dissipation can be induced, hence it is essential to quantify the pressure drop that is induced from all the cases for the design consideration. The pressure drop rises almost quadratically with *BR* because of inertial forces being especially significant at *BR* = 1. The enhancement of the heat transfer thus comes at the expense of a pressure drop, which might not be desirable. In the case of *BR* = 1.0 and Reynolds number of 7200, the penetration cooling length (PCL) and cooling angle (γ) are 3.0 and 9.3°, respectively, recording the best thermal performance among the cases. However, the pressure drop is as high as 2886.7 Pa/m, which is considerably significant in comparison to the other cases. Moreover, although reducing the BR can help in saving the pressure drop as shown in the case of BR = 7200, thermal performance degrades significantly, especially at Re = 1800.

Similarities in **Table 2**, redirect the discussion to other considerations in the design phase of the thermal management system using metal foam, such as the space and power consumption. For example, all cases have a similar trend of increasing penetration cooling length and decreasing cooling angle with increasing blockage ratio. However, the pressure drop increases with increasing BR, which is a trade-off that must be considered in the design process. **Table 2** shows that increasing the blockage ratio (BR) by 2.0 while keeping the Reynolds number constant results in an increase in pressure drop by a factor of 6.8 and an increase in heat transfer by a factor of 1.8. Moreover, increasing the Reynolds number by 3.0 while keeping the blockage ratio constant results in an increase in pressure drop by a factor of 14.9 and an increase in heat transfer by a factor of 2.9. Additionally, the space required for the metal foam must also be considered, as well as the power consumption of the fan or pump that is used to circulate the working fluid. Ultimately, the best design for a thermal management system will depend on the specific application and the desired trade-offs between thermal performance, space, and power consumption. To illustrate this, **Table 2** shows that if there is no space limitation for the thermal management design, the cooling design can be based on Case 01. However, if there is limited space for the metal foam, the design can be based on Case 05, which has nearly the same thermal performance and pressure drop. In the ultimate situation of a compact design, the design philosophy can be based on Case 08, which has nearly the same thermal performance but with a nearly two-fold higher pressure drop.

Figure 13 represents the distribution of the average $IHTC$ distribution along the streamwise direction and the normalised pressure drop to the base case (case 03) for three distinct cases: BR = 0.5 at Re = 7200, BR = 0.8 at Re = 3600, and BR = 1.0 at Re = 3600. Despite variations in the BR and Re number among these cases, their cooling angles and PCL were found to be closely aligned (see **Table 2**), resulting in analogous trends in the $IHTC$ distribution. It is noteworthy that the maximum $IHTC$ distribution occurs at the front face of the metal foam in **Figure 13** due to its exposure to high stream flow, prominently observed in the case of Re = 7200 for all cases. While the overall trends in $IHTC$ distribution appear to be similar, distinctive fluctuations are evident among the cases, exemplified by BR = 1.0 and Re = 3600. Remarkably, this case initiates with an initial $IHTC$ value of approximately 150 $\mathrm{W/m^2K}$ ranks second highest in magnitude and surpasses all other cases from the middle to the end of the metal foam. This confirms the significant impact of flow leakage on heat transfer. Despite the relatively lower Re number compared to the BR = 0.5 case, the full filling of channel by the metal foam enhances the $IHTC$ distribution, as it forces the flow to penetrate the porous zone entirely. Furthermore, a higher BR may not always guarantee the best thermal performance, as evidenced by BR = 0.5 with Re = 7200, which exhibits a lower pressure drop and relatively similar $IHTC$ distribution trend compared to that of BR = 0.8 with Re = 3600. Specifically, the mean $IHTC$ value for the case of BR = 0.5 and Re = 7200 is 133.21 $\mathrm{W/m^2K}$, whereas for BR = 0.8 and Re = 3600, it is 65.84 $\mathrm{W/m^2K}$. The substantial difference between these values can be attributed to the higher stream exposure at the front face, resulting in a higher mean value despite the relatively comparable trends and the amount of flow leakage in each case.

Table 2 Comparison of penetration cooling length, pressure drop and cooling angle for different simulation scenarios.

No	Blockage ratio & Reynolds number	Penetration cooling length (X/h)	Cooling angel (γ)	Pressure drop (dp/L_{Foam})	$IHTC$	dp/dp_o	Nu/Nu_o
01	BR = 0.5, Re = 7200	1.8	15.4°	446.7	78.4	14.9	2.9
02	BR = 0.5, Re = 3600	1.3	21.6°	115.0	46.2	3.8	1.7
03* **(Base case)**	**BR = 0.5, Re = 1800**	**0.8**	**30.0°**	**30**	**27.4**	**1.0**	**1.0**
04	BR = 0.8, Re = 7200	2.4	11.8°	1353.3	110.1	45.1	4.2
05	BR = 0.8, Re = 3600	1.8	15.5°	356.7	65.8	11.9	2.4
06	BR = 0.8, Re = 1800	0.9	27.0°	96.7	39.4	3.2	1.4
07	BR = 1.0, Re = 7200	3.0	9.3°	2886.7	133.2	96.2	4.9
08	BR = 1.0, Re = 3600	1.8	15.4°	753.3	81.0	25.1	2.9
09	BR = 1.0, Re = 1800	1.7	15.9°	203.3	48.1	6.8	1.8

***NOTE**: dp_o and Nu_o is calculated based on case 03 (BR = 0.5, Re = 1800) which has the lowest pressure drop and heat transfer performance

Based on **Figure 13** and **Table 2** it can be deduced that considering the constraints of available space and power consumption, there exist multiple scenarios for the design of thermal management systems using open-cell metal foam. In cases where spatial limitations are non-restrictive and the cooling fan's power can be augmented without bounds, a solution involving a high blockage ratio within the high Reynolds number regime could be pursued. Conversely, if spatial allowances are unlimited while power consumption remains a limiting factor in the design, an alternative approach involving a suitable combination of blockage ratio and Reynolds regime can be considered to meet the design criteria.

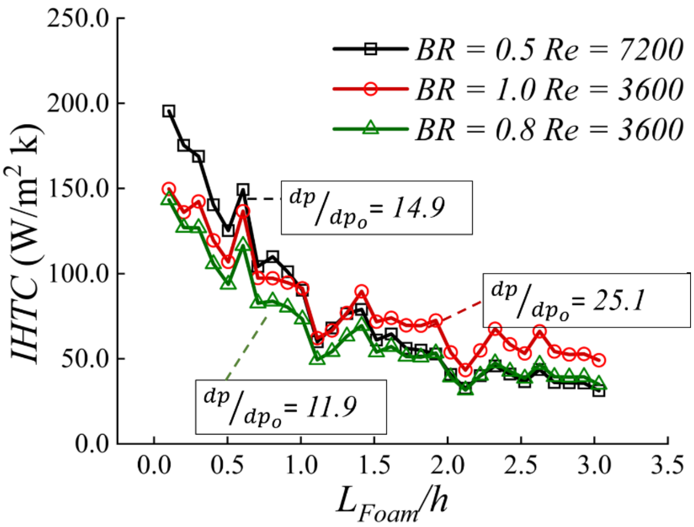

Figure 13 The average *IHTC* along the streamwise direction for different blockage ratios (BR) and Reynolds numbers (Re).

4 Conclusion

A pore-scale turbulence model was developed to investigate the complex flow in a composite porous-fluid system with stochastic open-cell metal foam. The study considered conjugate heat transfer and turbulent flow conditions. The primary focus was to understand the influence of different blockage ratios (BRs) and Reynolds number (Re) on both convective heat transfer and pressure drop phenomena. Moreover, important flow features, including flow leakage, the channelling effect, and thermal characteristics such as fluid and solid temperature distributions, were discussed. The findings of this study proposed a design strategy for thermal management systems while also providing a comprehensive description of flow behaviours and thermal characteristics at the pore-scale level. The following are the key conclusions that can be drawn from the findings of this investigation:

1. A new factor, the penetrating cooling length (PCL), has been introduced as a measure of the performance of the composite porous-fluid systems, along with the blockage ratio and Reynolds number. The PCL quantifies the portion of the porous ligaments that is not cooled or experiences deficient cooling. The results show that the PCL increases with increasing Reynolds number and blockage ratio.

2. Increases of Re number at BR = 0.5 minimise the amount of the flow that can leak from the porous block even if the leakage is more than 50% for all the Re numbers at 1.5h which is considered an early stage of the porous block. Moreover, an equal flow leakage has been observed from all the Re numbers at BR = 0.8 in which the dependency of Re number is no longer held when increasing the BRs. This behaviour can be attributed to the high momentum flow in the non-porous region serving as a resistive layer, forcing the flow to traverse its path inside the pores, thus minimizing leakage.

3. Increasing the blockage ratio has a drastic effect on the heat transfer, especially at the first part of the porous block and near the clear porous-fluid interface region, as observed in BR = 0.8 and BR = 1.0. Moreover, higher BR may not always guarantee the best thermal performance, as evidenced by BR = 0.5 with Re = 7200, which exhibits a lower pressure drop and a relatively similar $IHTC$ distribution trend compared to that of BR = 0.8 with Re = 3600. A correlation of IHTC is proposed based Reynolds number, blockage ratio and development length of the metal foam.

4. Flow leakage is significant at low blockage ratios and Reynolds numbers, and it is highly dependent on the Reynolds number. However, at high Reynolds numbers and blockage ratios, the high-momentum flow in the non-porous region forms a resistive layer at the porous-fluid interface, forcing the flow through the pores and minimizing leakage. Additionally, all Reynolds numbers exhibited the same level of flow leakage as the blockage ratios increased to BR = 0.8, at which point flow leakage is no longer dependent on the Reynolds number.

5. Doubling the blockage ratio at a constant Reynolds number increases the pressure drop by 6.8 times and the heat transfer by 1.8 times. Similarly, tripling the Reynolds number at a constant blockage ratio increases the pressure drop by 14.9 times and the heat transfer by 2.9 times.

6. The turbulent kinetic energy distribution within metal foam is influenced by its complex structure, with an increase in TKE especially noticeable at the foam's leading edge. The BR also affects TKE; higher BRs correlate with greater turbulence. Notably, at BR less than 1, two regions of interest emerge: a pronounced increase in TKE at the leading edge and a generated turbulence at the interface, most evident at x/h = 2. However, at a BR of 0.5, the TKE is significantly lower, leading to low flow velocity inside the pores and altered TKE distribution.

7. There is no single best design for a thermal management system with stochastic metal foam. The trade-off between thermal performance and pressure drop, which are influenced by the both blockage ratio and Reynolds number, must be considered for an effective design. In cases where spatial limitations are not restrictive and the cooling fan's power can be increased without bounds, a solution involving a high blockage ratio within the high Reynolds number regime could be pursued. Conversely, if spatial allowances are unlimited while power consumption remains a limiting factor in the design, an alternative approach involving a low blockage ratio within the low Reynolds regime can be considered based on the design philosophy.

Acknowledgement

This work was supported by the UK Engineering and Physical Sciences Research Council (EPSRC) [grant numbers EP/W033542/1]. Data supporting this publication can be obtained on request. The authors would like to acknowledge the assistance given by Research IT and the use of the Computational Shared Facility at The University of Manchester.

References

[1] W. Li, S. Guo, L. Tan, L. Liu, and W. Ao, "Heat transfer enhancement of nano-encapsulated phase change material (NEPCM) using metal foam for thermal energy storage," *International Journal of Heat and Mass Transfer,* vol. 166, p. 120737, 2021.

[2] X. Yang, P. Wei, X. Cui, L. Jin, and Y.-L. He, "Thermal response of annuli filled with metal foam for thermal energy storage: An experimental study," *Applied Energy,* vol. 250, pp. 1457-1467, 2019.

[3] X. Yang, J. Yu, Z. Guo, L. Jin, and Y.-L. He, "Role of porous metal foam on the heat transfer enhancement for a thermal energy storage tube," *Applied Energy,* vol. 239, pp. 142-156, 2019.

[4] K. Leong and L. Jin, "Effect of oscillatory frequency on heat transfer in metal foam heat sinks of various pore densities," *International Journal of Heat and Mass Transfer,* vol. 49, no. 3-4, pp. 671-681, 2006.

[5] M. M. Heyhat, S. Mousavi, and M. Siavashi, "Battery thermal management with thermal energy storage composites of PCM, metal foam, fin and nanoparticle," *Journal of Energy Storage,* vol. 28, p. 101235, 2020.

[6] S. Razza *et al.*, "Heat transfer performance of structured catalytic reactors packed with metal foam supports: Influence of wall coupling," *Catalysis Today,* vol. 273, pp. 187-195, 2016.

[7] V. V. Calmidi and R. L. Mahajan, "Forced convection in high porosity metal foams," *J. Heat Transfer,* vol. 122, no. 3, pp. 557-565, 2000.

[8] Z. He, Y. Yan, and Z. Zhang, "Thermal management and temperature uniformity enhancement of electronic devices by micro heat sinks: A review," *Energy,* vol. 216, p. 119223, 2021.

[9] K. Nilpueng, L. G. Asirvatham, A. S. Dalkılıç, O. Mahian, H. S. Ahn, and S. Wongwises, "Heat transfer and fluid flow characteristics in a plate heat exchanger filled with copper foam," *Heat and Mass Transfer,* vol. 56, pp. 3261-3271, 2020.

[10] S. Mancin, C. Zilio, A. Cavallini, and L. Rossetto, "Pressure drop during air flow in aluminum foams," *International Journal of Heat and Mass Transfer,* vol. 53, no. 15-16, pp. 3121-3130, 2010.

[11] D. Y. Kim and K. C. Kim, "An experimental study on the thermal and hydraulic characteristics of open-cell nickel and copper foams for compact heat exchangers," *International Journal of Heat and Mass Transfer,* vol. 130, pp. 162-174, 2019.

[12] T. De Carvalho, H. Morvan, D. Hargreaves, H. Oun, and A. Kennedy, "Pore-scale numerical investigation of pressure drop behaviour across open-cell metal foams," *Transport in Porous Media,* vol. 117, pp. 311-336, 2017.

[13] M. Nazari, D. J. Vahid, R. K. Saray, and Y. Mahmoudi, "Experimental investigation of heat transfer and second law analysis in a pebble bed channel with internal heat generation," *International Journal of Heat and Mass Transfer,* vol. 114, pp. 688-702, 2017.

[14] A. Hamadouche, R. Nebbali, H. Benahmed, A. Kouidri, and A. Bousri, "Experimental investigation of convective heat transfer in an open-cell aluminum foams," *Experimental Thermal and Fluid Science,* vol. 71, pp. 86-94, 2016.

[15] M. Nazari, M. Ashouri, M. H. Kayhani, and A. Tamayol, "Experimental study of convective heat transfer of a nanofluid through a pipe filled with metal foam," *International Journal of Thermal Sciences,* vol. 88, pp. 33-39, 2015.

[16] T. Dixit and I. Ghosh, "An experimental study on open cell metal foam as extended heat transfer surface," *Experimental Thermal and Fluid Science,* vol. 77, pp. 28-37, 2016.

[17] P. Singh, K. Nithyanandam, and R. L. Mahajan, "An experimental and numerical investigation of forced convection in high porosity aluminum foams subjected to jet array impingement in channel-flow," *International Journal of Heat and Mass Transfer,* vol. 149, p. 119107, 2020.

[18] Z. Nie, Y. Lin, and Q. Tong, "Numerical investigation of pressure drop and heat transfer through open cell foams with 3D Laguerre-Voronoi model," *International Journal of Heat and Mass Transfer,* vol. 113, pp. 819-839, 2017.

[19] X. Bai, F. Kuwahara, M. Mobedi, and A. Nakayama, "Forced convective heat transfer in a channel filled with a functionally graded metal foam matrix," *Journal of Heat Transfer,* vol. 140, no. 11, p. 111702, 2018.

[20] M. Jadidi, H. K. Param, A. Revell, and Y. Mahmoudi, "Flow leakage and Kelvin–Helmholtz instability of turbulent flow over porous media," *Physics of Fluids,* vol. 34, no. 10, 2022.

[21] F. S. Anuar, I. A. Abdi, and K. Hooman, "Flow visualization study of partially filled channel with aluminium foam block," *International Journal of Heat and Mass Transfer,* vol. 127, pp. 1197-1211, 2018.

[22] M. Jadidi, H. K. Param, A. Revell, and Y. Mahmoudi, "Large eddy simulations of turbulent heat transfer in packed bed energy storage systems," *Journal of Energy Storage,* vol. 59, p. 106449, 2023.

[23] A. Kopanidis, A. Theodorakakos, E. Gavaises, and D. Bouris, "3D numerical simulation of flow and conjugate heat transfer through a pore scale model of high porosity open cell metal foam," *International Journal of Heat and Mass Transfer,* vol. 53, no. 11-12, pp. 2539-2550, 2010.

[24] X. Chu, W. Wang, G. Yang, A. Terzis, R. Helmig, and B. Weigand, "Transport of turbulence across permeable interface in a turbulent channel flow: interface-resolved direct numerical simulation," *Transport in Porous Media,* vol. 136, pp. 165-189, 2021.

[25] U. Guide, "StarCCM+ version 2020.1," *SIEMENS simcenter,* 2020.

[26] T.-H. Shih, W. W. Liou, A. Shabbir, Z. Yang, and J. Zhu, "A new k-ϵ eddy viscosity model for high reynolds number turbulent flows," *Computers & Fluids,* vol. 24, no. 3, pp. 227-238, 1995.

[27] S. Mancin, C. Zilio, A. Diani, and L. Rossetto, "Air forced convection through metal foams: Experimental results and modeling," *International Journal of Heat and Mass Transfer,* vol. 62, pp. 112-123, 2013.

[28] Á. Hernández, "Combined flow and heat transfer characterization of open cell aluminum foams," *University of Puerto rico, Mayagüez campus,* 2005.

[29] R. Byron Bird, W. E. STEWARD, and E. N. Lightfoot, "Transport Phenomena," John Wiley & Sons, 1960.

[30] F. P. Incropera, D. P. DeWitt, T. L. Bergman, and A. S. Lavine, *Fundamentals of Heat and Mass Transfer*. Wiley New York, 1996.

[31] E. C. Nsofor and G. A. Adebiyi, "Measurements of the gas-particle convective heat transfer coefficient in a packed bed for high-temperature energy storage," *Experimental Thermal and Fluid Science,* vol. 24, no. 1-2, pp. 1-9, 2001.

[32] F. Kuwahara, M. Shirota, and A. Nakayama, "A numerical study of interfacial convective heat transfer coefficient in two-energy equation model for convection in porous media," *International Journal of Heat and Mass Transfer,* vol. 44, no. 6, pp. 1153-1159, 2001.

[33] X. Nie, R. Evitts, R. Besant, and J. Bolster, "A new technique to determine convection coefficients with flow through particle beds," *Journal of Heat Transfer,* vol. 133, no. 4, 2011.

[34] M. Jadidi, A. Revell, and Y. Mahmoudi, "Pore-scale large eddy simulation of turbulent flow and heat transfer over porous media," *Applied Thermal Engineering,* vol. 215, p. 118916, 2022.

[35] M. Jadidi, H. K. Param, and Y. Mahmoudi, "On the mechanism of turbulent heat transfer in composite porous-fluid systems with finite length porous blocks: Effect of porosity and Reynolds number," *International Journal of Heat and Mass Transfer,* vol. 208, p. 124006, 2023.

[36] Y. Kuwata, "Direct numerical simulation of turbulent heat transfer on the Reynolds analogy over irregular rough surfaces," *International Journal of Heat and Fluid Flow,* vol. 92, p. 108859, 2021.